# Stretch bending – the plane within the sheet where strains reach the forming limit curve

**F M Neuhauser[1,2], O R Terrazas[1], N Manopulo[2], P Hora[2], and C J Van Tyne[1]**

[1] Advanced Steel Processing and Products Research Center, Colorado School of Mines, 920 15th St, Golden, CO 80401 USA
[2] Institut für virtuelle Produktion, Department of Mechanical and Process Engineering, Swiss Federal Institute of Technology, ETH Zurich, Tannenstrasse 3, 8092 Zürich, Switzerland

E-mail: cvantyne@mines.edu

**Abstract**. Finite element analysis (FEA) was used to model the angular stretch bend test, where a strip of sheet metal is locked at both ends and a tool with a radius stretches and bends the center of the strip until failure. The FEA program used in the study was Abaqus. The FEA model was verified by experimental work using a dual phase steel (DP600) and with a simplified analytical analysis. The FEA model was used to simulate the experimental test for various frictional conditions and various radii of an upward moving tool. The primary objective of the study was to evaluate the concave-side rule, which states that during stretch bending the forming limit occurs when the strains on the concave surface plane of the bent sheet (i.e. bottom plane) reach the forming limit curve (FLC). The verification with experimental data indicates that the FEA model represents the process very well. Only conditions where failure occurred on or near the tooling are included in the results. The FEA simulations showed that the actual forming limit of the sheet occurs when the strains on the bottom plane of the sheet (i.e. concave side of the bend) reach the forming limit curve for high friction and small tool radii. For lower friction and for larger tool radii the actual forming limit occurs when strains on other planes in the sheet (i.e. mid planes or top surface plane) reach the forming limit curve. The implications of these results suggest that care must be taken in assessing forming operations when both stretch and bending occur. Although it is known that the FLC cannot predict the forming limit for small bend radii, the common assumption that the forming limit occurs when the strains for the middle thickness plane of the sheet reach the forming limit curve or that the concave side rule is often made. Understanding the limits of this assumption needs to be carefully and critically evaluated.

## 1. Introduction

The forming limit diagram (FLD) is commonly used in the forming industry to predict localized necking in sheet metals. However experimental and mathematical determination of forming limit curves is based on in plane deformation without taking a bending component into account. In this paper the question is addressed whether a forming limit diagram predicts localized necking too conservative or too late for different amounts of superimposed bending for different strain conditions ranging from plane strain to uniaxial strain. This knowledge is of importance in finding tools, which do not cause failure during production in deep drawing processes via finite element simulations, especially for die and punch radii where bending is superimposed on a stretching component.

Since the forming limit diagram is only valid for membrane deformation *i.e.* from Keeler and Brazier's forming limit curve [1], Tharrett and Stoughton [2] introduced the so called concave-side rule which states, that in bending with tension deformation the neck occurs on the convex-side of the sheet, when the strains on the concave-side reach the plane-strain forming limit. Therefore, Tharrett and Stoughton could detect a clear enhanced formability of stretch bend operations in comparison to in plane only stretch deformation. However, when compared to previous studies, the localization effect seems to dominate the enhancement of formability since shear fracture is still present.

Enhanced formability due to bending could also be found by Atzema et al. [3] who performed Nakazima tests with different punch radii. The smaller the radii, the higher was the observed formability. The effect was highest in plane strain and negligible in the uniaxial region.

Kitting et al. [4] applied the concave-side rule on H340LAD materials and found, that it predicts the formability well for punch radii $R \geqslant 10$ mm and underestimates material formability for $R < 10$ mm. Further, Kitting et al. [5] expanded the experimental characterization of bending under tension for not only plane strain, but also uniaxial and biaxial strain states.

These previous studies show that bending can enhance the formability of sheet metal, where this enhancement is defined as strains that are above the forming limit curve. From a practical perspective, this enhancement of formability might be exploited during some sheet forming operations. In order to use this extra level of formability requires a better understand of the bending effect.

During stretching and bending the neck formation will be observed on the top (i.e. tensile side due to bending) side of the sheet. The enhancement will allow this top surface to have higher strains than predicted by the forming limit curve. It would be expected that some plane within the thickness of the sheet will be at the forming limit when the top surface experiences a local neck. The objective of the present study was to examine via finite element analysis the angular stretch bend test to determine which plane in the sheet metal reaches the forming limit strain when localization of strain on the top surface occurs during the test.

Although there have been extensive studies reported in the literature on sheet bending under tension, the present investigation as well as the previous studies on the bending enhancement of formability use an angular stretch bend test which is different from the traditional bending under tension test methods. In the traditional test, the sheet metal with some back tension bends onto a roller, slides over the roller and unbends as it comes off the roller. In the angular stretch bend test the tooling simultaneously stretches and bends the sheet without the bending onto and off of a roller. The mechanics and stress states in the sheet are different for these two types of tests.

## 2. Experimental Procedure

Experimental angular stretch bend tests were performed on DP600. Figure 1 shows a photo and a schematic of the angular stretch bend test. The sheet specimens were 180 mm in length, 25 mm wide and 1.45 mm thick. The lubrication used was Teflon (PTFE) with LPS2 lubricant. The tool geometry was punch radii of 1, 2.5 and 5 mm, die entry radius of 4.7 mm, drawbead radius of 3.2 mm, distance between drawbeads 95 mm, and die opening 76.2 mm. The punch velocity was 5.08 mm/s

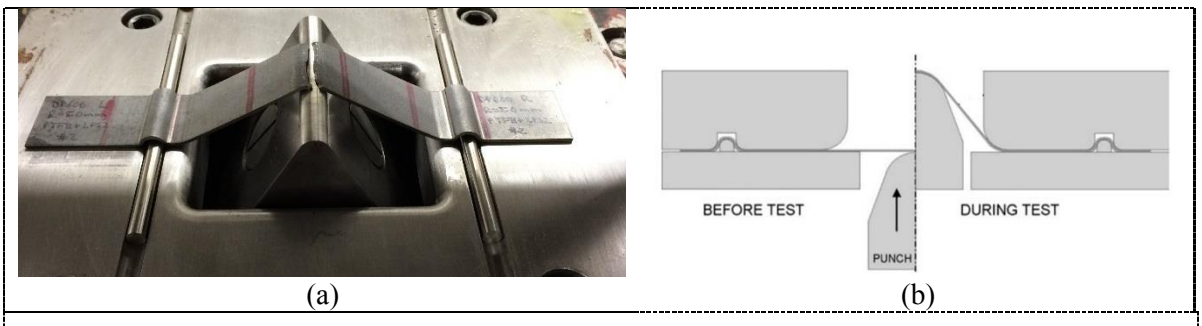


**Figure 1.** Angular stretch bend test (a) photograph, (b) schematic.

The tests were run to fracture. Force was measured during the test. The localization of strain was assumed to occur at the maximum force in the force displacement curve.

For the finite element analysis a mixed Hockett-Sherby and Gosh yield curve was used as the constitutive model for the DP600 based on tensile test data. Four tensile tests were performed for DP600 sheet steel in rolling direction at an engineering strain rate of 0.002 1/s in order to describe the material's static stress response in the elastic region and also the hardening in the plastic region. An isotropic hardening model was used in the present study.

Young's modulus was calculated to be E = 195,100 MPa as the mean value of the four tensile tests. A Poisson's ratio of 0.3 is assumed in the elastic region of the flow curve.

In order to determine the dependency of flow stress on the equivalent plastic strains in the plastic part of the flow curve, the following steps were conducted:

1) Engineering stress – strain curve truncated at the uniform elongation strain
2) Removal of the elastic part of engineering stress – strain curve
3) Conversion to true stress – logarithmic strain curve
4) Subtract elastic component of logarithmic strains
5) Fit the experimental true stress – plastic logarithmic strain curve to the Hockett-Sherby hardening law (using a least square fit)
6) Fit the experimental true stress – plastic logarithmic strain curve to the Gosh hardening law (using a least square fit)
7) Fit the last 40 data points of the experimental true stress – plastic logarithmic strain curve to a mixed Hockett-Sherby Gosh hardening law (using a least square fit) which corresponds to a strain range of about 0.08 – 0.12
8) Average all three obtained flow curves

The reason for the rather complicated Hockett-Sherby Gosh fit is that strains occurring in the stretch bend simulation are well beyond the uniform elongation strains. Therefore, it is of crucial importance that the flow curve does not only match the experimental data before the uniform elongation, but also accurately predicts material flow behavior for strains exceeding uniform elongation. The mixed Hockett-Sherby Gosh approach enables the possibility to best capture the slope of the last 40 experimental data points, which correspond to the last 0.04 strain and therefore delivers a reasonable extrapolated region. The constitutive equations are as follows:

$$\sigma_{HS} = A_1 - (A_1 - B_1) * e^{(-m_1 * \varepsilon^{n_1})} \quad (1)$$

$$\sigma_G = A_2 * (B_2 + \varepsilon)^{n_2} - C_2 \quad (2)$$

$$\sigma_{HS-G} = \kappa * \sigma_{HS} + (1 - \kappa) * \sigma_G \quad (3)$$

Equation (1) is the Hockett-Sherby model, Equation (2) is the Gosh model, and Equation (3) is the mixed model. Table 1 gives the model parameters used.

**Table 1** – Parameters for the Mixed Hockett-Sherby Gosh Yield Curve

| $\kappa$ [] | $A_1$ [MPa] | $B_1$ [MPa] | $m_1$ [] | $n_1$ [] | $A_2$ [MPa] | $B_2$ [MPa] | $n_2$ [] | $C_2$ [MPa] |
|---|---|---|---|---|---|---|---|---|
| 0.54 | 855.92 | 406.77 | 7.26 | 0.69 | 1102.1 | 0.0025 | 0.17 | 0 |

The general purpose software ABAQUS 6.14-1 was used to model the angular stretch bend test. A three dimensional model was implemented, where the tools, including die, holder and punch, are represented by analytical rigid body surfaces. To expand the experimental work, punch radii of 1, 2.5, 5, 10, 15 and 20 mm were used to set the sheet under tension with different superimposed bending components from mild to severe.

The blank was rendered by 3D linear 8 node brick elements with reduced integration (1 integration point per element instead of 2 in each direction) to avoid shear locking. Eleven elements were used through the thickness. Due to symmetry a one-quarter blank was modelled and the blank was locked in position at the drawbeads. The friction coefficient is held constant between the holder and sheet as

well as between the die and sheet at a value of 0.18. In order to vary the strain paths at the punch nose, the friction coefficient between punch and sheet is varied between 0.0, 0.03, 0.07, 0.15 and 0.2.

An analytical model, based on the assumption of homogenous strains along the ligament and homogenous strains through the thickness was used to verify the finite element results.

In order the compare the strains of the angular stretch bend test sample in different layers of the sheet with forming limits, the FLD introduced by Keeler and Brazier [1] was calculated. The empirical equations consist of a forming limit in plane strain, $FLD_0$ as:

$$\mathrm{FLD}_0^{\mathrm{true}} = \ln\left[1 + (23.3 + 14.14 * \mathrm{t}) * \left(\frac{\mathrm{n_t}}{0.21*100}\right)\right], \mathrm{n_t} \leqslant 0.21 \quad (4)$$

which is dependent on the n value in the Hollomon hardening law and the sheet thickness t. The left side of the forming limit diagram decreases linearly with $\varepsilon_{\mathrm{minor}}$ while the right side is a function of a logarithm depending on the values of $FLD_0$ and $\varepsilon_{\mathrm{minor}}$ as:

$$\varepsilon_{\mathrm{maj}} = \ln\left[0.6 * (e^{\varepsilon_{\mathrm{min}}} - 1) + e^{\mathrm{FLD}_0^{\mathrm{true}}}\right], \varepsilon_{\mathrm{min}} > 0 \quad (5)$$

## 3. Results and Discussion

Figure 2 shows the FEA simulation results compared to the analytical verification and the experimental results. Figure 2a shows a good correspondence between the analytical analysis and the homogeneous portions of the force-displacement curves. The analytical model does not account for localization so there is a difference when the finite element simulations begin to exhibit localized deformation. The analytical model is for the ligament region only, so the model does not have a dependence on the radius of the tooling. Figure 2b shows the comparison of the finite element simulations with no friction and the experimental results with the use of Teflon lubrication. The comparison is quite good. These two verification steps provide good confidence in the finite element simulations, which will be used to determine the plane in the sheet that reaches the forming limit when localization occurs.

Since the scope of the current study was to access the strains in the sample when localized necking occurs and then to compare these strains with a conventional FLC, the punch displacement is needed, where the top surface of the sheets starts to localize. The load maximum generally signals the onset of diffuse necking, not localized necking. However, for a plane-strain condition, localized and diffuse necking fall together to be seen i.e. in the modified maximum force criteria by Hora et al. [6] that extends the maximum force criteria to access localized necking strains.

Three kinds of results where extracted from each FEA simulation: strain paths at the punch nose in different layers of the sheet, major and minor strains along the ligament, also in different layers of the sample and forming limits of the center line when the local neck arises. Figure 3 shows the location of the three surfaces in the sheet from which the strain paths were extracted. Figure 4 shows the strain paths for different surfaces in the steel using two different punch radii. The surfaces are at the punch nose where strain localization would occur. The friction coefficient was 0.03. The touching surface is the surface that reaches the traditional FLC when the localization starts. In Figure 4(a) the touching surface is between the middle surface and the bottom surface and the top surface can accommodate strains well above the FLC before localization occurs. In contrast Figure 4(b) for a larger punch radius the touching surface is between the middle surface and the top surface and the top surface has less strain at localization as compared to the deformation with a 1 mm punch radius. The other results were used to obtain a better understanding of the plane in the sheet that reaches the forming limit;

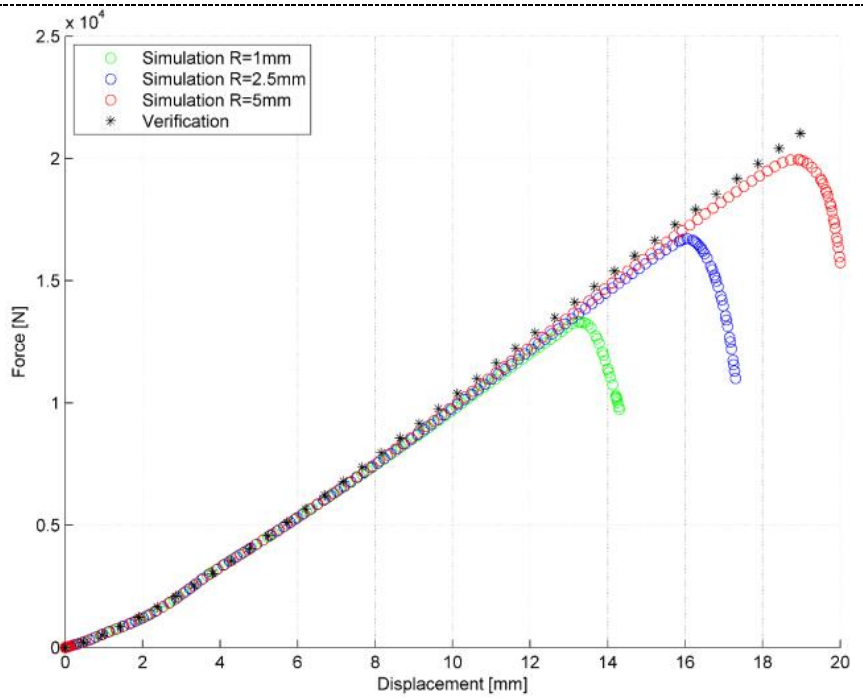


(a)

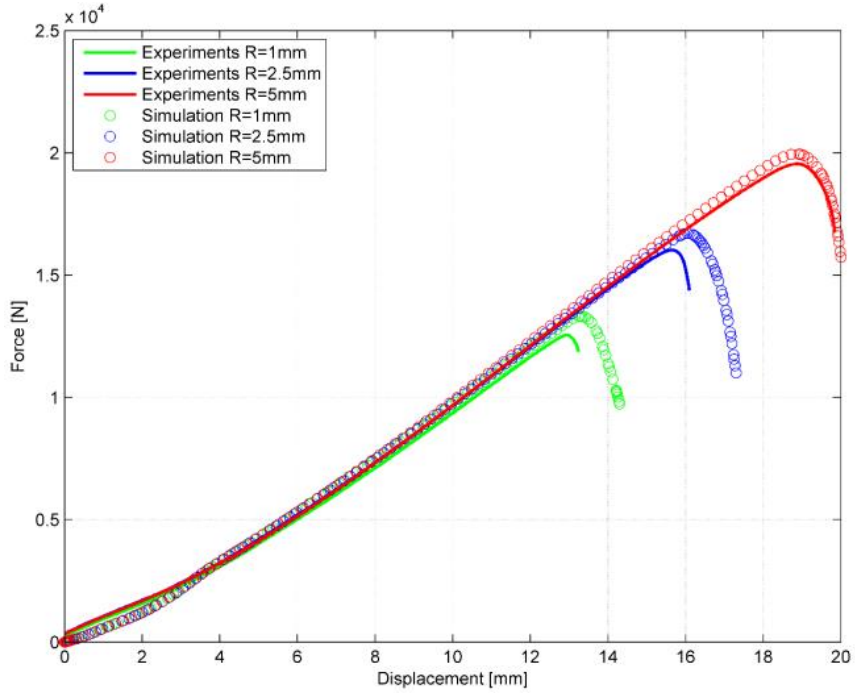


(b)

**Figure 2.** Verification of finite element model (a) with analytical solution, where the finite element results are shown by open circles and the analytical solution is shown by the black circles (b) with experiments, where the finite element results are shown by the open circles and the experimental results are the solid lines.

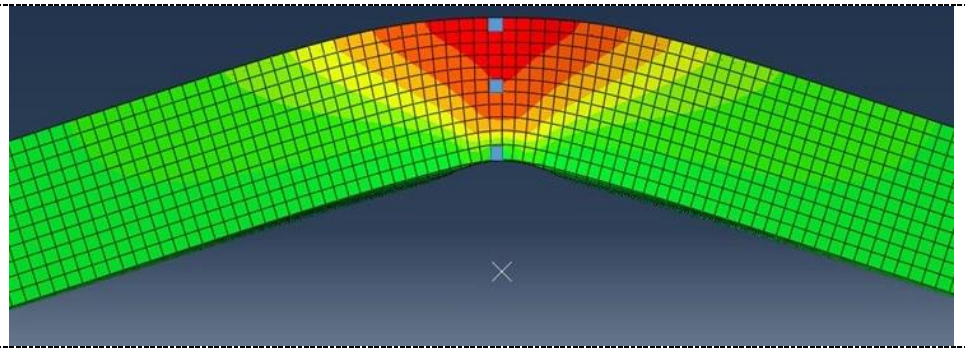

**Figure 3.** Top, middle and bottom surfaces where strains paths were extracted.

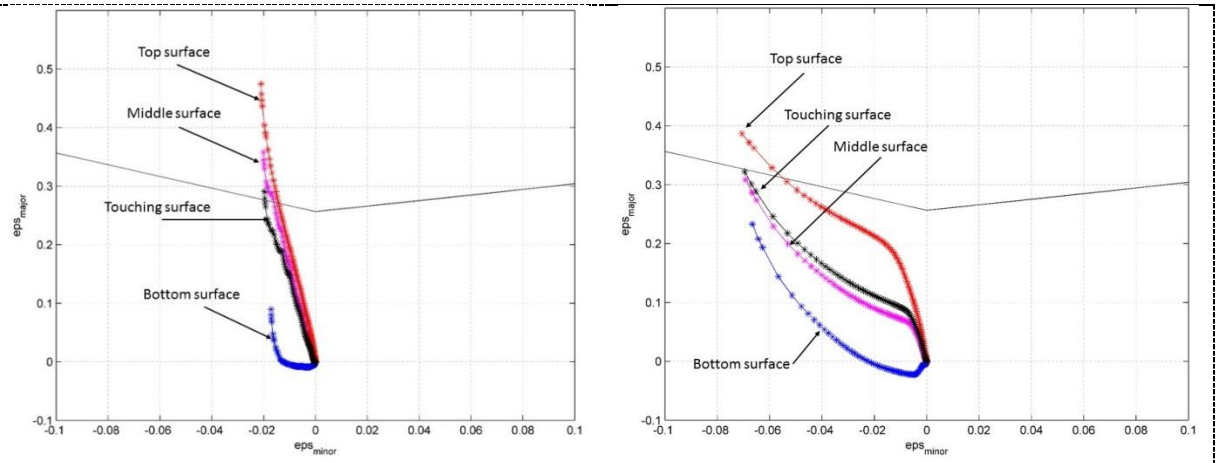


**Figure 4.** Strain paths for different sheet surfaces at the punch nose (a) with a tooling punch radius of 1 mm, (b) with a tooling punch radius of 5 mm. The top, middle and bottom surfaces of the sheet are tracked in these figures. The touching surface is the one that comes in contact with the FLC at the limit point during the test.

Figure 5 shows the sheet on the 2.5 mm punch at the last stable time increment in the simulation. As can be observed the strains are highly concentrated in the top region of the sheet. Localization of the deformation is observed by the slight valley that is seen in this top region.

Table 2 gives a summary of the position of the sheet plane that touches the FLC when localization occurs. The (–) / (+) means that the touching plane is slightly below/above the respective plane. At large radii and high friction there is sufficient restraint so that necking and a tensile failure occurs in the ligament region rather than on the punch nose. The bending enhanced formability occurs with small punch radii. The results are consistent with the concave-side rule of Tharrett and Stoughton [2] since they used small punch radius and no lubrication. The results in this study show that the concave side rule is valid for limited conditions.

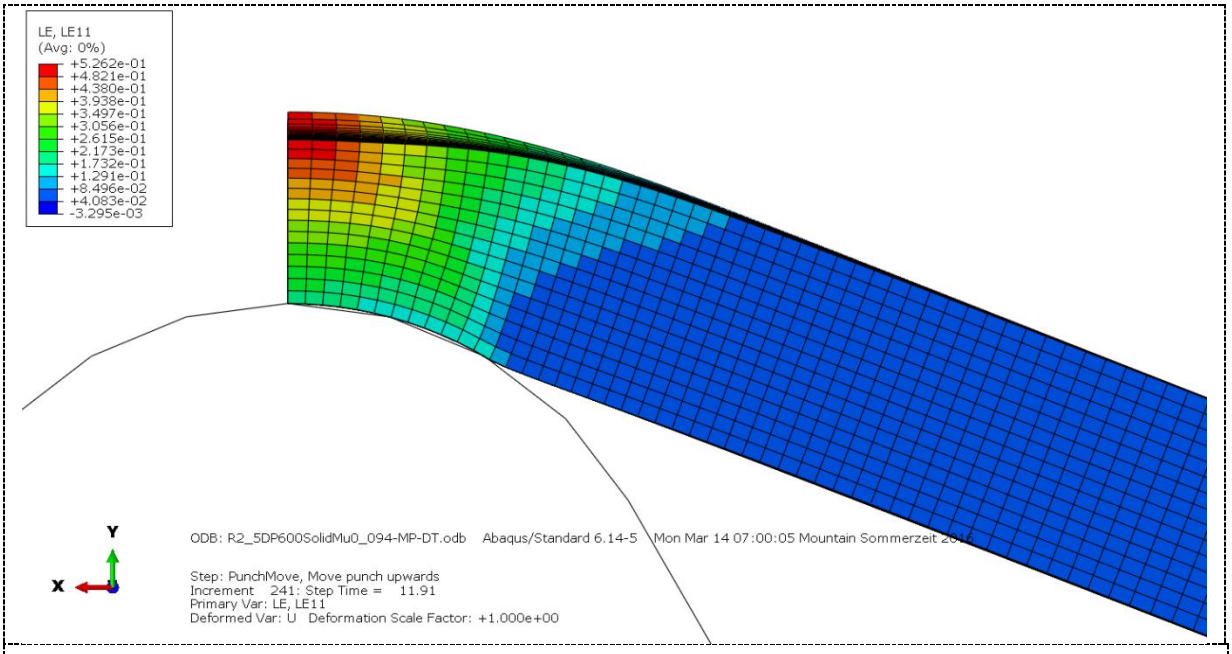


**Figure 5.** Sheet on the 2.5 mm punch radius at the last stable time increment. Localized necking has started

**Table 2** – Summary of Touching Planes in Every Simulation

| Punch Radius | μ = 0.00 | μ = 0.03 | μ = 0.07 | μ = 0.15 | μ = 0.20 |
|---|---|---|---|---|---|
| R = 1 mm | Mid (-) | Mid (-) | Bottom (+) | Bottom (+) | Bottom (+) |
| R = 2.5 mm | Mid | Mid | Mid | Mid | Mid |
| R = 5 mm | Mid (-) | Mid (+) | Mid (+) | Mid (+) | NL |
| R = 10 mm | Top | Top | Top | NL | NL |
| R = 15 mm | Top | Top (+) | Top (+) | NL | NL |
| R = 20 mm | Top (+) | Top (+) | NL | NL | NL |

NL = Necking in ligament

Although both the friction and bend radius influence the location of the failure, examination of Table 2 shows that the value of the coefficient of friction plays a small role in controlling the plane that reaches the formability limit. The punch radius has a more dominant role. It is also observed that the touching plane is lower in the sheet with the smaller punch radius, which indicates that the enhancement of formability due to bending is greater when there is a small radius involved with the bending. Because of the small radius and the very low friction, it is likely that this enhancement of formability could have some use in actual sheet forming operations. Nevertheless, a study, which provides a better quantification of the bending enhancement of formability, can be performed.

## 4. Summary

The results of the current study show that the plane within the sheet that reaches the traditional FLC can vary depending on the bending radius and the frictional conditions. The bending radius has a much greater effect as compared to friction. At small bending radii the plane that touches the FLC is pushed further from the top surface of the sheet toward the bottom. The concave-side rule of Tharrett and Stoughton occurs with small punch radius and high friction. The common assumptions that the

forming limit occurs when the strains for the middle thickness plane of the sheet reach the forming limit curve or that the concave side rule is universally applicable need to be carefully and critically evaluated for the specific forming conditions.

**Acknowledgements**
We thank the Advanced Steel Processing and Products Research Center (ASPPRC) at Colorado School of Mines for partial support for this project

**References**
[1] Keeler S P and Brazier W G 1997 Relationship between Laboratory Material Characterization and Press-Shop Formability *Microalloying 75 Proc.* 517
[2] Tharrett M R and Stoughton T B 2003 Stretch-Bend Forming Limits of 1008 AK Steel *Soc. Automot. Eng.* 123
[3] Atzema E H, Fictorie E, van den Boogaard A H and J. M. M. Droog J M M 2010 The influence of curvature on FLC's of mild steel, (A)HSS and aluminium *Int. Deep Draw. Res. Group, IDDRG*
[4] Kitting D, Koplenig M, Ofenheimer A, Pauli H and Till E T 2009 Application of a 'concave-side rule' approach for assessing formability of stretch-bent steel sheets *Int. J. Mater. Form.* **2** 427
[5] Kitting D, Ofenheimer A, Pauli H and Till E T 2011 Experimental Characterization of Stretch-Bending Formability of AHSS Sheets," *AIP Conf. Proc.* **1353** 1589
[6] Hora P, Tong L and Berisha B 2013 Modified maximum force criterion, a model for the theoretical prediction of forming limit curves *Int. J. Mater. Form.* **6** 267